Spacecraft Doppler tracking: Noise budget and accuracy achievable in precision radio science observations

S. W. Asmar and J. W. Armstrong

Jet Propulsion Laboratory, California Institute of Technology, Pasadena, California, USA

L. Iess

Dipartimento di Ingegneria Aerospaziale e Astronautica, Università di Roma "La Sapienza," Rome, Italy

P. Tortora

II Facoltà di Ingegneria, Università di Bologna, Forlì, Italy

Received 1 June 2004; revised 11 November 2004; accepted 21 December 2004; published 15 March 2005.

[1] We discuss noise in Doppler tracking of deep space probes and provide a detailed noise model for Doppler radio science experiments. The most sensitive current experiments achieve fractional frequency fluctuation noise of about 3×10^{-15} at 1000-s integration time, corresponding to better than 1 micron per second velocity noise. Our noise model focuses primarily on the Fourier range $\approx 10^{-4}$–1 Hz, but we briefly discuss noise in lower-frequency observations. We indicate applications of the noise model to experiment planning, identify phenomena limiting current Doppler sensitivity, and discuss the prospects for significant sensitivity improvements.

Citation: Asmar, S. W., J. W. Armstrong, L. Iess, and P. Tortora (2005), Spacecraft Doppler tracking: Noise budget and accuracy achievable in precision radio science observations, *Radio Sci.*, *40*, RS2001, doi:10.1029/2004RS003101.

1. Introduction

[2] All deep space probes have communications systems used for both control of the probe from the ground, via the uplink, and for return of telemetry from the probe, via the downlink. These communications systems typically serve at least two additional purposes: navigation, using observations of the radio ranging and Earth-spacecraft Doppler to determine probe position and velocity, and radio science, using the radio links explicitly for mission science return. Radio science studies have been historically diverse including investigations such as determination of planetary masses and mass distributions, measurement of planetary atmospheres, ionospheres, and rings, estimation of planetary shapes, studies of the solar wind, and precision tests of relativistic gravity. Radio science observations, depending on the phenomena being investigated, involve measurement and study of the radio amplitude, phase, and polarization over a variety of timescales. For an overview of radio science observations and instrumentation, see *Asmar and Renzetti* [1993].

0048-6604/05/2004RS003101$11.00

[3] Common to these diverse scientific objectives, however, is the need to understand the noises limiting the observations. In this paper, we examine the noise in precision Doppler tracking observations and provide a detailed noise model for Cassini-era Doppler radio science. We also identify phenomena limiting the Doppler sensitivity and comment on upgrades which would significantly improve performance. The paper is organized as follows: in section 2 we briefly review the Doppler tracking measurement method. In section 3, we discuss the principal noises affecting Doppler observations on timescales $\approx 1-10^4$ s. In section 4 we give the transfer functions of these noises to the Doppler observable. Section 5 contains a brief discussion of noise sources important for longer-duration ($>10^4$ s) Doppler observations. Section 6 discusses the limits of current sensitivity and the prospects for significant future improvements.

2. Doppler Measurements

[4] Doppler tracking observations conceptually seek to measure the relative velocity of the Earth and a spacecraft by comparing the frequency of the radio signal received from the spacecraft with the frequency of a ground-based

reference signal. When the signal transmitted by the spacecraft is derived from an onboard oscillator (e.g., an ultrastable oscillator), the measurement is said to be "one-way." If the spacecraft transponds a signal transmitted from the ground and the ground-based reference for the Doppler is the same one that drives the transmitter, the observation is "two-way." The measurement is "three-way" if the ground station receives a signal transponded by the spacecraft but the uplink is from a different ground station. These distinctions are relevant because, depending on the Doppler mode, both signals and noises have different transfer functions connecting them to the observation. The observation can be expressed as y(t), a time series of fractional Doppler fluctuations, that is the change in frequency between the received and reference signals, divided by the nominal frequency, f_0, of the Doppler link. This time series contains both signal and noise components. In what follows, we use T_1 and T_2 to be the one-way (downlink) and two-way light times, respectively.

3. Principal Noises in the Doppler Observations

[5] Nonsignal disturbances in a Doppler link are due to instrumental noises (random errors introduced by ground or spacecraft themselves), propagation noises (random frequency/phase fluctuations caused by refractive index fluctuations along the line of sight), or systematic errors. Instrumental noises include phase fluctuations associated with finite signal-to-noise ratio (SNR) on the radio links, ground and spacecraft electronics noise, unmodeled bulk motion of the spacecraft or ground station, frequency standard noise (ground standards and, in one-way observations, the spacecraft oscillator to which the downlink is referenced), and antenna mechanical noise (unmodeled phase variation within the ground station). Propagation noise is caused by phase scintillation as the radio wave passes through the troposphere, ionosphere, and solar wind. Instrumental and propagation noises display varying degrees of nonstationarity.

[6] These disturbances enter the Doppler time series through transfer functions [*Estabrook and Wahlquist*, 1975; *Wahlquist et al.*, 1977; *Tinto*, 1996, 2002; *Abbate et al.*, 2003]. The aggregate time series, $y(t) = \Delta f(t)/f_0$, can be modeled as the sum of linear operations on the signals and the noises. If "*" indicates convolution, we view the time series as y(t) = (signal * signal transfer function) + Σ (noise_i * transfer function for noise_i). Below we will show that most of the variability of the time series can be explained by a few principal noises. All real experiments also have (ideally low-level) systematic effects, e.g., bias of the Doppler frequency due to systematic errors in the removal of the spacecraft orbital signature or systematic errors in calibrations. With the exception of a short discussion of low-frequency noise (section 4) we do not address systematic effects in this paper.

[7] Transfer functions are discussed in section 4. In what follows we first give statistics of the raw noises in terms of power spectra of fractional frequency fluctuations $S_y(f)$, (which is by convention "two-sided," meaning that the variance is the integral of $S_y(f)$ from minus infinity to infinity) and Allan deviation, a time domain measure of fractional frequency fluctuation as a function of averaging time. Explicitly, the Allan deviation, $\sigma_y(\tau)$, is the structure function of locally time-averaged fractional frequency fluctuations [*Barnes et al.*, 1970]:

$$\sigma_y^2 = \frac{1}{2}\langle|\overline{y(t)} - \overline{y(t+\tau)}|^2\rangle = \int_{-\infty}^{\infty} df\, 2S_y(f)\sin^4(\pi f\tau)/(\pi f\tau)^2 \quad (1)$$

with

$$\overline{y(t)} = \int_{t'}^{t'+t} y(t')dt' \quad (2)$$

3.1. Instrumental Noises

[8] Fluctuations in phase, thus $\Delta f/f_0$, occur due to finite SNR on the radio links. These white phase noise, thus blue frequency noise, fluctuations are dominated by the lowest SNR element in the link. In current two-way observations, this is the SNR of the downlink. The level is instrumentation- and range-dependent, but given roughly by $\sigma_y(\tau) \sim 10^{-16}$ (1000 s/τ) for typical Cassini cruise observations (and $\tau \gg$ reciprocal bandwidth used to detect the phase).

[9] Ground and spacecraft electronics noise do not dominate current-era observations. Transponder noise is measured on the ground to be typically 10^{-15} or smaller; the Cassini Ka band frequency translator was as low as 2×10^{-16}, (transponders based on digital architectures generally have poorer stability). Aggregate ground instrumental noise due to the exciter, transmitter, or receiver has been measured in zero two-way light time tests to be $<3 \times 10^{-16}$ at τ = 1000 s. Because the two-way light time, T_2, is 0 in these tests the frequency and timing system (FTS) contribution cancels and must be measured independently. A power spectrum of ground instrumental noise test data is given in the work of *Abbate et al.* [2003, Figure 1].

[10] Unmodeled motions of the spacecraft or ground station introduce Doppler noise. Motion of the spacecraft can be independently determined with Cassini by mon-

itoring the attitude and control system on the spacecraft [*Won and Lee*, 2001]. Spectra measured for $f > 0.0001$ Hz show that Cassini spacecraft motion noise contributes $<3 \times 10^{-16}$ at $\tau \approx 1000$ s. Noise spectra of spacecraft motion have not been independently measured in the 10^{-4}–10^{-6} Hz band. However, the excellent sensitivities of the Cassini Solar Conjunction Experiment [*Bertotti et al.*, 2003] and the Cassini Gravitational Wave Experiment [*Armstrong et al.*, 2003] in the $\tau \sim 10^5$–10^6 s range suggests very low noise level. Attributing all residual low frequency fluctuation observed in the gravitational wave experiment to spacecraft motion gives a few parts in 10^{15} as a very conservative upper limit to Cassini motion noise in the microhertz band. Although intrinsically small, ground antenna motion noise at $\tau \sim 1000$ s can be a leading disturbance in the Doppler link. Differential measurements of 34-m (diameter) Deep Space Network (DSN) antennas against (presumably more stable) small antennas suggest ground antenna mechanical noise of $< 4 \times 10^{-15}$ at $\tau \sim 1000$ s under favorable conditions [*Otoshi and Franco*, 1992; *Rochblatt et al.*, 1999]. Antenna mechanical noise can also be isolated or bounded in *operational* data based on its transfer function [*Wahlquist et al.*, 1977; *Armstrong*, 1998]. This gives one-way noise as small as 2×10^{-15} under benign conditions from observations on a new 34 m beam waveguide antenna taken at high-elevation angle during quiet winter nights at the NASA/JPL Goldstone CA tracking site [*Armstrong et al.*, 2003] and an upper bound of $\approx 10^{-14}$ for operational observations on the NASA/JPL 34 m high-efficiency subnet, at night with high elevation [*Armstrong*, 1998]. Observations under less benign conditions presumably give poorer performance, but antenna mechanical noise has not been quantitatively studied under all operational conditions.

[11] Frequency and timing system (FTS) noise is fundamental to Doppler tracking observations and depends strongly on the hardware providing the frequency reference. Ground-based FTS systems (e.g., hydrogen masers) achieve stability better than 10^{-15} at $\tau = 1000$ s [*Kuhnle*, 1989]. In one-way observations, spacecraft ultrastable oscillators (USO) achieve much poorer sensitivity, typically $\approx 10^{-13}$ for 1000 s integration times. (For observations requiring one-way mode, e.g., for simplicity of data interpretation, this 10^{-13} USO stability is considered superior in the category of spaceborne oscillators.)

3.2. Propagation Noise

[12] Radio waves propagating through media with random refractive index fluctuations develop phase/frequency fluctuations. Deep space probe radio links pass through the troposphere, ionosphere, and solar wind. At microwave frequencies, tropospheric refractive index fluctuations are nondispersive and dominated by water vapor fluctuations [e.g., *Resch et al.*, 1984; *Armstrong and Sramek*, 1982; *Keihm*, 1995; *Keihm et al.*, 2004]. From a yearlong study of zenith water vapor fluctuations (the "wet" component of tropospheric phase scintillation) the average statistics show seasonal fluctuation being higher in summer daytimes and lowest in winter nighttimes. The level of the scintillation is variable, bounded roughly by 3–30×10^{-15} at $\tau \sim 1000$ s for winter nighttime observations (Table 1). Dry component fluctuations are smaller; *Keihm et al.* [2004] show spectra of wet and dry components down to $f \sim 10^{-6}$ Hz. Wet component scintillations can be largely ($\approx$90% at low Fourier frequencies under favorable conditions) removed using water vapor radiometer–based "advanced media calibration" instrumentation [*Resch et al.*, 2002; *Tanner and Riley*, 2003]; this instrumental upgrade has significantly improved the sensitivities of several Cassini radio science investigations [*Bertotti et al.*, 2003; *Armstrong et al.*, 2003; *Kliore et al.*, 2005]. Dry component fluctuations are usually calibrated based on surface metrology, the assumption that the atmosphere is in hydrostatic equilibrium, and a model for the elevation dependence of the dry troposphere. The calibrations were especially useful in summer daytime conditions where, after plasma calibration, troposphere is a leading noise source. Figure 1 illustrates Doppler residuals (here expressed as two-way range-rate residuals: $\Delta v = 0.5\ c\ \Delta f/f_0$) measured during the Cassini solar conjunction period in June 2002 before and after wet tropospheric calibrations.

[13] At wavelength λ, the refractive index fluctuations in the ionospheric and solar wind plasmas are proportional to λ^2. Because of this dispersive characteristic, raw plasma scintillation is much weaker for deep space radio links using, e.g., Ka band ($\approx$32 GHz) rather than S band ($\approx$2.3 GHz). Dispersion also allows isolation of the plasma scintillation in multilink observations. The Viking orbiters had dual S and X band downlinks, designed such that the downlink X band phase was 11/3 times the downlink S band phase. From differential S − (3/11)X phase measurements, the one-way (downlink) plasma could be isolated, independent of any nondispersive effects (e.g., tropospheric scintillation, motion of the spacecraft, FTS noise). Note that implicit in this is the assumption that the two links propagate on the same line of sight and thus respond to the same plasma fluctuations. For microwave frequencies and for propagation in the solar wind, this is a good approximation except perhaps for ray paths passing very close to the Sun where differential refraction causes the ray paths to differ slightly at the two frequencies. At meter wavelengths, this has been exploited to measure the solar wind velocity from the time-of-crossing of irregularities across the two sightlines [*Scott et al.*, 1983].

Table 1. Representative Noise Sources and the Corresponding Allan Deviation[a]

Noise Source	Allan Deviation at 1000 s (Two-Way Unless Noted)	Comments/References
Ground FTS (including distribution)	<1E-15	*Kuhnle* [1989]
USO	≈1E-13 (one-way)	test data from *Asmar et al.* [2003]
Antenna mechanical noise	<4E-15 (favorable conditions)	DSS-25 measured 3.6E-15 under static conditions at elevation = 47 degrees [*Rochblatt et al.*, 1999]; DSS-13 measured <3.1E-15 under static conditions at elevation = 37 and 46 degrees [*Otoshi and Franco*, 1992]; DSS-15, 45, 65 measured <1E-14 under operational conditions with antenna moving [*Armstrong*, 1998]; and DSS-25 < 3E-15 for winter/nighttime [*Armstrong et al.*, 2003]
Ground electronics (excludes FTS)	2.3E-16	DSS-25 test data with antenna stationary on 2001 days of year 152–153 [*Abbate et al.*, 2003]
Plasma phase scintillation at Ka band	<1E-15 for Sun-Earth-spacecraft angles >160 deg	*Armstrong et al.* [1979] and Figure 2
Cassini spacecraft motion ("buffeting")	2.6E-16	*Won and Lee* [2001]
Thermal noise (finite SNR in the link)	∼1E-16	depends on link SNR and configuration; general formula in the work of *Barnes et al.* [1970] for white phase noise
Cassini Ka band translator noise (transponder)	<1.7E-15	prelaunch tests show ≈1E-16 with −127 dBm signal input level; in-flight determination by L. Iess: <1.7E-15 using method of *Bertotti et al.* [1993] to isolate Ka band translator
Raw tropospheric scintillation	<3E-15 to 30E-15 (Goldstone winter/night; highly variable)	*Keihm* [1995], *Keihm et al.* [2004], and *Armstrong and Sramek* [1982]
Tropospheric scintillation after AMC calibration	<1.5E-15 (favorable conditions); ≈3.2E-15 (median conditions in AMC/CEI tests)	*Resch et al.* [2002], comparing AMC and CEI data; median improvement after applying AMC corrections was factor of 2.8

[a]DSS, deep space station, numeric designation of antenna in the Deep Space Network; CEI, connected element interferometer; AMC, advanced media calibration system.

[14] Figure 2 shows the power spectral density of one-way plasma phase scintillation versus the Sun-Earth-spacecraft angle. The open circles in this figure show differential observations (received S band phase − (3/11) of the received X band phase) of the Viking spacecraft, expressed as S_y(0.001 Hz) and taken over a wide range of Sun-Earth-spacecraft (elongation) angles [*Woo and Armstrong*, 1979; *Armstrong et al.*, 1979]. Because these are differential measurements, they essentially reflect the equivalent one-way S band plasma phase scintillation on the downlink. The crosses are similarly the equivalent one-way X band plasma scintillation noise determined from Cassini gravitational wave experiment data taken near opposition in 2001–2003. For Cassini the X and Ka band downlinks are coherent with the X band uplink. The crosses are derived from differential X − (880/3344) Ka phase observations. The curve through the S band data is an idealized model assuming that the spacecraft is ≥1 AU from the Earth and that the scintillation comes from a radially directed, constant-velocity solar wind. It also ignores aberration due to the relative motion of the Earth and spacecraft; see *Armstrong et al.* [1979]. In the relevant geometrical optics limit, plasma phase fluctuations are the sight-line integral of $(2\pi/\lambda)$ (refractive index fluctuation), the RMS plasma phase scintillation

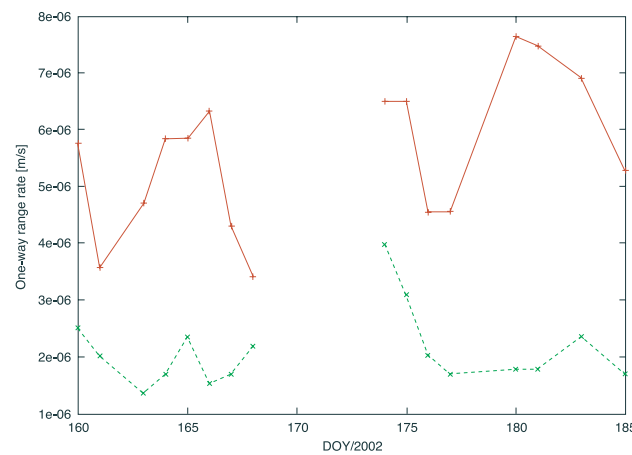

Figure 1. Range rate residuals measured during Cassini solar conjunction in June 2002. Upper and lower curves show 300-s average RMS value of residuals before and after wet tropospheric calibrations respectively. Data were precalibrated for plasma noise using the multi-frequency link scheme.

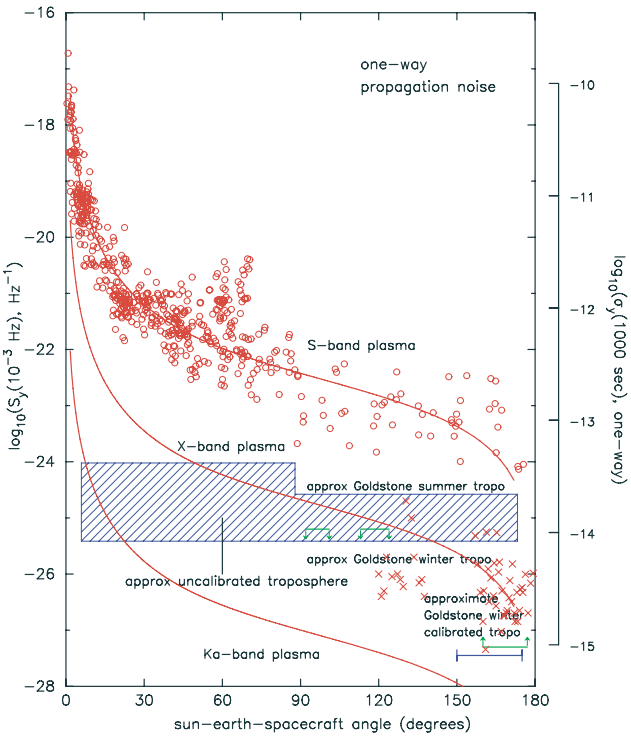

Figure 2. Power spectral density of one-way plasma phase scintillation at $f = 0.001$ Hz versus Sun-Earth-spacecraft angle (red circles for S band and red crosses for X band), approximate level of uncalibrated tropospheric scintillation noise (blue area), and limits to antenna mechanical noise (green). The right-hand scale is the equivalent Allan deviation at 1000-s integration time, assuming a Kolmogorov (S_y proportional to $f^{-2/3}$) spectral shape.

varies as λ and thus $S_y(f)$ varies as λ^4. The curves labeled X and Ka bands are scaled this way from the S band model curve. We note that the crosses (X band data) agree well with the X band curve scaled from the S band model. Shown on the right hand side is the equivalent $\sigma_y(1000\ s)$, assuming the refractive index fluctuations have a Kolmogorov spectrum. That is, the right-hand scale is derived from the left-hand scale according to equation (1) under the assumption that $S_y(f) = \text{constant}\ f^{-2/3}$.

[15] As indicated above, if differential S-X or X-Ka downlinks are available, the downlink plasma contribution can be estimated and removed. More elaborate radio systems allow estimation and removal of the plasma scintillation on both the up and the down links. For example, the Cassini spacecraft can operate 5 links simultaneously: X up, Ka up, X down coherent with the X up, Ka down coherent with the X up, and Ka down coherent with the Ka up [*Kliore et al.*, 2005]. Suitable linear combinations of the data can almost perfectly cancel all plasma scintillation [*Iess et al.*, 1999; *Tortora et al.*, 2002, 2003; *Iess et al.*, 2003; *Bertotti et al.*, 2003; *Tortora et al.*, 2004]. Using this multilink configuration, the Doppler accuracy at conjunction (shown in Figure 1) is almost identical to the one attainable at opposition. The principal propagation noises near solar opposition and their Allan deviations at $\tau = 1000$ s are shown in Table 1, updated from *Abbate et al.* [2003].

4. Transfer Functions

[16] Transfer functions of the noises to the Doppler data depend on the observing mode. In what follows we subscript y(t) to indicate the type of Doppler observed: $y_1(t)$ and $y_2(t)$ are one- and two-way observations respectively. The transfer function is zero for cases such as the spacecraft transponder in a one-way mode. Table 2 shows the time domain transfer functions (i.e., the function which is convolved with the noise) for the principal noises. These are expressed here in the time domain, but it is often useful to restate them in the frequency domain. For example, in a two-way observation antenna mechanical noise is convolved with $\delta(t) + \delta\ (t - T_2)$. Thus the spectrum of antenna mechanical noise in the two-way Doppler observable is the product of the raw

Table 2. Time-Domain Doppler Transfer Functions[a]

Noise Source	One-Way Transfer Function[b]	Two-Way Transfer Function
Ground FTS (including distribution)	$\delta(t)$	$\delta(t) - \delta(t - T_2)$
USO	$\delta(t - T_1)$	N/A
Antenna mechanical noise	$\delta(t)$	$\delta(t) + \delta(t - T_2)$
Ground electronics (excludes FTS)	$\delta(t)$	depends on component
Plasma phase scintillation (x = distance to plasma blob)	$\delta(t - x/c)$	$[\delta(t - x/c) + \delta(t - T_2 + x/c)]$
Spacecraft motion ("buffeting")	$\delta(t - T_1)$	$2\delta(t - T_1)$
Thermal noise (finite SNR in the link)	$\delta(t)$	$\delta(t)$
Transponder noise	N/A	$\delta(t - T_1)$
Raw tropospheric scintillation	$\delta(t)$	$\delta(t) + \delta(t - T_2)$
Tropospheric scintillation after AMC calibration	$\delta(t)$	$\delta(t) + \delta\ (t - T_2)$

[a] T_1, one-way light time; T_2, two-way light time; unity transponder ratio assumed.

[b] All modulus squared = 1.

mechanical noise spectrum and 4 $\cos^2(\pi f T_2)$. The positive correlation at the two-way light time causes the effective mechanical noise spectrum to have nulls. At and near these frequencies other antenna mechanical noise becomes secondary and, in some applications, this can be exploited to improve SNR [e.g., *Estabrook and Wahlquist*, 1975; *Tinto and Armstrong*, 1998].

[17] As an example, the important special case of two-way Doppler has noise part of the time series well-approximated by

$$\begin{aligned} y_2(t) &= \Delta f(t)/f_0 \\ &= \text{solar wind plasma}(t) * [\delta(t - x/c) + \delta(t - T_2 \\ &\quad + x/c)] + \text{ionospheric plasma}(t) * [\delta(t) \\ &\quad + \delta(t - T_2)] + \text{troposphere}(t) * [\delta(t) + \delta(t - T_2)] \\ &\quad + \text{ground station antenna mechanical}(t) \\ &\quad * [\delta(t) + \delta(t - T_2)] + \text{FTS}(t) * [\delta(t) - \delta(t - T_2)] \\ &\quad + \text{thermal noise}(t) + \text{spacecraft transponder}(t) \\ &\quad * \delta(t - T_1) + 2[\text{spacecraft buffeting}(t)] \\ &\quad * \delta(t - T_1) \end{aligned} \tag{3}$$

where x is the distance from the tracking station to a solar wind blob and T_2 is the two-way light time from the tracking station to the spacecraft and back.

[18] Figure 3 shows the two-sided power spectrum of two-way fractional Doppler frequency residuals, $S_{y2}(f)$, computed from data taken at DSS-25 during the 2001–2002 Cassini solar opposition [*Armstrong et al.*, 2003]. Residuals were determined after removal of the systematic orbital Doppler shift due to the spacecraft trajectory and after correcting for both the (small) solar opposition plasma scintillation effect using the Cassini multilink radio system [*Bertotti et al.*, 2003] and tropospheric scintillation using the advanced media calibration system. Because the data are corrected for plasma phase scintillation, the spectrum shown in Figure 3 contains contributions only from nondispersive noise processes. The observations spanned 40 days and thus had intrinsic frequency resolution of about 0.3 μHz; the spectrum in Figure 3 has been smoothed to a resolution bandwidth of about 7 μHz to reduce estimation error and make it easier to see transfer function effects in the spectrum.

[19] At high frequencies ($f > 10^{-4}$ Hz) the noise budget presented here accurately describes the principal features of the spectrum. Up to about $10^{-2.5}$ Hz, the plasma- and troposphere-corrected continuum is dominated by a random process having correct level and spectral signature for antenna mechanical noise. In Figure 3 the periodic modulation of the spectrum ($\cos^2$ nulls at odd multiples of $1/(2T_2)$) at high frequencies is evident. This is the signature of either antenna mechanical noise or residual tropospheric noise (i.e., residual after calibration of the tropospheric effect by the water vapor radiometer–based advanced media calibration (AMC) system). In pre-experiment verification tests of the AMC [*Resch et al.*, 2002] the AMC-measured tropospheric phase fluctuations were compared with simultaneous interferometric phase fluctuations in a tropospheric noise–dominated short-baseline connected-element radio interferometer (CEI). Those tests showed the AMC calibrations significantly improved the quality of the CEI data (see also Figure 1). The level of the observed cosine-squared-modulated spectrum in Figure 3 is too high to be reasonably ascribed to residual tropospheric calibration error, but is consistent with estimates of antenna mechanical noise in this band. Thermal noise and FTS noise also contribute (minor, in the case of Cassini, but potentially significantly for other spacecraft observations) noise power in Figure 3.

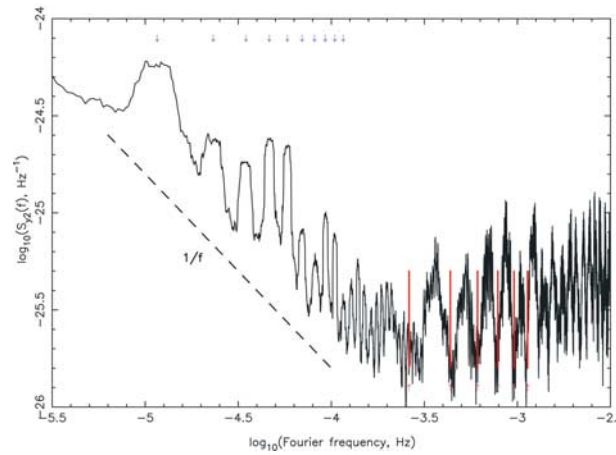

Figure 3. Spectrum of two-way fractional Doppler fluctuations, corrected for plasma and tropospheric fluctuations, taken during the 2001–2002 Cassini gravitational wave experiment smoothed to a frequency resolution of ≈7 μHz. The frequencies of 1 cycle/sidereal day and nine harmonics are marked with the blue arrows. Six frequencies of the nulls of the antenna mechanical noise transfer function $k/(2T_2)$, where k is an odd integer and T_2 is the average two way light time over the observations (5730 s), are marked with the red lines.

[20] The timescales of interest in some radio science investigations [e.g., *Bertotti et al.*, 2003] extend to frequencies lower than 0.0001 Hz. Noise in the low-frequency (10^{-6} to 10^{-4} Hz) Doppler band has not been as well-studied, however. In this band, S_{y2} from Cassini Gravitational Wave Experiment 1 [*Armstrong et al.*, 2003] can be used as an example of the aggregate achievable sensitivity. From Figure 3, below about 0.0001 Hz S_{y2} is roughly a 1/f continuum, plus spectral lines near one cycle per day and its harmonics. (A 1/f spectrum of Doppler noise corresponds to a f^{-3} spectrum

of displacement noise, i.e., a very red displacement spectrum.) The total variance of y_2 between 10^{-6} to 10^{-4} Hz is about 3×10^{-29} corresponding to root mean square path length variation on timescales $\approx 10^4 - 10^6$ s of about 2 cm. At these Fourier frequencies two-way Cassini observations are operating in the "long-wavelength limit" (LWL: $1/f \gg T_2$):

$$S_{y2} \rightarrow 4\pi^2 T_2^2 f^2 S_y^{FTS}(f) + S_y^{s/c\ motion}(f) + S_y^{s/c\ elect}(f) + S_y^{ground\ elect}(f) + 4S_y^{tropo}(f) + 4S_y^{ant}(f)$$

[21] From the viewpoint of isolating noises, this is unfortunate. The contributions to S_{y2} from the main noise processes mostly lose their signatures so it is difficult to ascribe features in the spectrum to specific causes. In the absence of spectral signatures, we attempt only to see if the observed variance is consistent with the variance expected from known noises. In the LWL, two-way FTS noise is suppressed by $4\ \pi^2\ f^2\ T_2^2$ and the (already small) frequency and timing noise does not contribute much variance to the low-frequency spectrum. Noise spectra of spacecraft motion, spacecraft electronics, and ground electronics noise have not been independently measured in the 10^{-4}–10^{-6} Hz band. However unless there are significant changes in the spectral shapes of these noises below 0.0001 Hz, they also probably do not contribute significantly at low frequencies in Figure 3. Spectra presented by *Keihm et al.* [2004] show that postcalibration tropospheric wet component fluctuations probably contribute less than 10% of the $f < 0.0001$ Hz variance in Figure 3. Antenna mechanical variability in the 10^{-4}–10^{-6} Hz band is probably a combination of both systematic and random effects. We view the following processes as approximately random: stochastic wind loading of the antenna, atmospheric pressure loading of the station, differential thermal expansion of the structure, uncompensated gravity loading of the antenna with the elevation angle. Systematic errors include imperfect subreflector focusing and low-level systematic imperfections in the support structure of the antenna. Response of the antenna structure to thermal changes ($\approx$10 K ambient temperature variations over a track driving a steel structure) can plausibly explain only a few millimeters of radio path length variation. The subreflector is continuously repositioned to compensate for elevation angle–dependent antenna distortions and keep the antenna in focus; systematic errors of a few millimeters due to imperfect focusing over an eight-hour track are not unreasonable. Additionally, systematic height variations in the azimuth track on which the antenna rolls can cause path length variability and, with reproducible systematic focusing errors, are candidate contributors for at least the 1 cycle/day line in the spectrum shown in Figure 3. Approximately 1 cm low-frequency path variability can plausibly be "explained" by aggregate unmodeled random and systematic motion within the ground antenna. In addition to intrastation motion variability, motion of the ground under the station will contribute variance at low frequencies. From VLBI error budgets, time-dependent station displacement noise of $\approx$1 cm due to atmospheric loading and other position variations of the ground are expected in this band [e.g., *Sovers et al.*, 1998]. These add only to about one-half of the observed low-frequency variance in Figure 3, however. This lack of quantitative agreement suggests either an additional unknown effect or imperfect current understanding of the spectra and level of the known low-frequency noise processes.

5. Prospects for Sensitivity Improvement

[22] Two-way Doppler experiments under favorable conditions currently achieve 3×10^{-15} at 1000 s integration. Particularly for measurement of relativistic effects, sensitivity improvements by one order of magnitude would be useful. Improving the aggregate system sensitivity by one order of magnitude would require bringing the noise level of each principal component down to about 1×10^{-16}. FTS stability would have to be improved by less than or about 1 order of magnitude, an amount that is probably consistent with near-term trends in timekeeping technology. Calibrated tropospheric noise would have to be similarly improved, either through instrumental upgrades, observations at sites more benign than Goldstone, or through use of coordinated listen-only observations made with stations at high altitude. (A procedure for doing this was independently proposed by F. B. Estabrook and R. W. Hellings in the context of improving Doppler tracking gravitational wave experiments.). Plasma scintillations noise can be mitigated by higher-frequency observations or by using multilink Cassini-style radio systems to estimate and remove it. Spacecraft positions noise would have to be only modestly improved over Cassini measurements. Antenna mechanical noise, however, would have to be improved by more than an order of magnitude. A partial solution, useful for only some types of observations, might be to take data only in the nulls of the cosine-squared two-way transfer function. A more general solution might involve independent high sampling rate monitoring of the antenna (e.g., metrology of the dish structure sufficient to calibrate or estimate/remove antenna mechanical effects or extraction of a small fraction of the uplink beam energy to compare against a very stable mechanical reference for the metrology correction).

Although challenging, improvement of Doppler sensitivity by at least one order of magnitude is probably technically possible.

6. Application: Observation Planning

[23] In addition to utility in designing signal processing procedures [e.g., *Armstrong*, 1998], noise budgets given here can be used to make tradeoffs in the planning of future radio science experiment such as those proposed by the community as summarized in the work of *Asmar et al.* [2002]. As specific examples, we consider Doppler tracking of a mission to Jupiter's satellite Europa to search for a subsurface ocean, or a mission to Mercury to measure its gravity harmonics and general relativity parameters.

[24] Pictures from the Galileo mission show that Europa has a young ice surface, perhaps only 1 km thick in places. Internal heating of Europa due to flexing by tide-raising forces could melt the underside of the icepack. Given the possibility of liquid water under the ice, there is the exciting possibility of life there. Hence the presence or absence of a subsurface ocean is of considerable interest. For the candidate mission described in the ''Europa Orbiter Mission and Project Description'' document, it is estimated that 2-way X band Doppler of 0.1 mm/s ($1\sigma,\tau$ = 60 s) over 3 Europa ''days'' (1 Europa day = 3.55 Earth days) would be required to detect a possible ocean. This corresponds to 6.7×10^{-13} in the two-way Doppler, at 60 s integration. To compare this with the noise from interplanetary and tropospheric scintillation (Figure 2), we assume a Kolmorgorov spectrum and scale to τ = 1000 s: $(1000/60)^{-1/6}\, 6.7 \times 10^{-13} = 4 \times 10^{-13}$. Thus from Figure 2, the mission should be designed so that the X band data are taken with SEP greater than about 20 degrees and tropospheric calibration should not, in this case, be required to meet the specification. (Of course observational margin and the possibility of detecting more subtle signals in the data would accrue with multilink observations and tropospheric calibration.)

[25] ''Geodesy'' and fundamental physics measurements at Mercury require very accurate orbit determination. The estimation of the relevant physical quantities (spherical harmonics, parameterized post-Newtonian constants of relativistic gravity) will be based almost exclusively on range and Doppler observables determined from microwave links between Earth and spacecraft. It is expected (BepiColumbo Mission Requirements Document issue 3, SCI-PB/RS/465, December 2003) that Doppler data with accuracy $\approx$1.5 microns/s (τ = 1000 to 10,000 s) is required to meet the desired accuracy in the ''geophysical'' and relativistic parameters. This corresponds to Allan deviations of about 10^{-14}. Because of the orbit of Mercury, these observations will necessarily be made at very small Sun-Earth probe angles. From Figure 2, even a two-way Ka band link would not meet this specification very close to the Sun. A multilink plasma cancellation system (e.g., like Cassini's) could calibrate plasma noise to 10^{-14}, even very close to the Sun. Note that in this case tropospheric scintillation correction would also be required to achieve 1.5 micron/s velocity error.

7. Summary

[26] We have developed a noise budget for current-era precision Doppler tracking of deep space probes. Our approach was to characterize both the raw noise statistics and the transfer functions relating these noises to the Doppler observable. Using Cassini observations we showed that appropriately calibrated Doppler data can achieve Allan deviations of a few times 10^{-15} for integration times $\sim$1000 s. We outlined the utility of this error budget in mission planning and the instrumental improvements required for order-of-magnitude improvements over the current capability.

[27] **Acknowledgments.** For SWA and JWA the research described here was carried out at the Jet Propulsion Laboratory, California Institute of Technology, under a contract with the National Aeronautics and Space Administration. The work of LI and PT has been funded by the Italian Space Agency (ASI).

References

Abbate, S. F., et al. (2003), The Cassini gravitational wave experiment, *Proc. SPIE*, *4856*, 90–97.

Armstrong, J. W. (1998), Radio wave phase scintillation and precision Doppler tracking of spacecraft, *Radio Sci.*, *33*, 1727–1738.

Armstrong, J. W., and R. A. Sramek (1982), Observations of tropospheric phase scintillation at 5 GHz on vertical paths, *Radio Sci.*, *17*, 1579–1586.

Armstrong, J. W., R. Woo, and F. B. Estabrook (1979), Interplanetary phase scintillation and the search for very low-frequency gravitational radiation, *Astrophys. J.*, *230*, 570–574. (Correction, *Astrophys. J.*, *240*, 719, 1980.)

Armstrong, J. W., L. Iess, P. Tortora, and B. Bertotti (2003), Stochastic gravitational wave background: Upper limits in the 10^{-6}–10^{-3} Hz band, *Astrophys. J.*, *599*, 806–813.

Asmar, S. W., and N. A. Renzetti (1993), The Deep Space Network as an instrument for radio science research, *JPL Publ.*, *80-93*.

Asmar, S., et al. (2002), Radio science and the Deep Space Network: Present and future, in *The Future of Solar System Exploration, 2003–2013—Community Contribution to the NRC Solar System Exploration Decadal Survey*, *Conf. Proc.*, vol. 272, edited by M. V. Sykes, pp. 355–359, Astron. Soc. of the Pac., San Francisco, Calif.

Asmar, S., D. Atkinson, M. Bird, and G. Wood (2003), Ultrastable oscillators for radio science investigations on plane-

tary entry probes, paper presented at International Workshop on Planetary Probe Atmospheric Entry and Descent Trajectory Analysis and Science, Eur. Space Ag., Lisbon, Portugal, 6–9 Oct.

Barnes, J. A., et al. (1970), Characterization of frequency stability, *NBS Tech. Note 394*, 48 pp.

Bertotti, B., G. Comoretto, and L. Iess (1993), Doppler tracking of spacecraft with multifrequency links, *Astron. Astrophys.*, *269*, 608–616.

Bertotti, B., L. Iess, and P. Tortora (2003), A test of general relativity using radio links with the Cassini spacecraft, *Nature*, *425*, 374–376.

Estabrook, F. B., and H. D. Wahlquist (1975), Response of Doppler spacecraft tracking to gravitational radiation, *Gen. Relativ. Gravitation Proc. Int. Conf.*, *6*, 439–447.

Iess, L., G. Giampieri, J. D. Anderson, and B. Bertotti (1999), Doppler measurement of the solar gravitational deflection, *Classical Quantum Gravity*, *16*, 1487–1502.

Iess, L., et al. (2003), The Cassini solar conjunction experiment: A new test for general relativity, *Proc. IEEE Aerospace Conf.*, *1*, 205–211.

Keihm, S. J. (1995), Water vapor radiometer measurements of the tropospheric delay fluctuations at Goldstone over a full year, *TDA Prog. Rep. 42-122*, pp. 1–11, NASA, Greenbelt, Md.

Keihm, S. J., A. Tanner, and H. Rosenberger (2004), Measurements and calibration of tropospheric delay at goldstone from the Cassini media calibration system, *IPN Prog. Rep. 42-158*, NASA, Greenbelt, Md.

Kliore, A. J., et al. (2005), Cassini radio science, *Space Sci. Rev.*, in press.

Kuhnle, P. F. (1989), NASA/JPL Deep Space Network frequency and timing, in *Proceedings of the Twenty-first Annual Precise Time and Time Interval (PTTI) Applications and Planning Meeting*, pp. 479–490, Storming Media, Washington, D. C.

Otoshi, T. Y., and M. M. Franco (1992), DSS-13 beam waveguide antenna frequency stability, *TDA Prog. Rep. 42-110*, pp. 151–159, NASA, Greenbelt, Md.

Resch, G. M., D. E. Hogg, and P. J. Napier (1984), Radiometric correction of atmospheric path length fluctuations in interferometric experiments, *Radio Sci.*, *19*, 411–422.

Resch, G. M., et al. (2002), The media calibration system for Cassini radio science, part III, *IPN Prog. Rep. 42-148*, pp. 1–12, NASA, Greenbelt, Md.

Rochblatt, D. J., P. H. Richter, and T. Y. Otoshi (1999), A microwave performance calibration system for NASA's Deep Space Network antennas, part 2: Holography, alignment, and frequency stability, in 10th *International Conference on Antennas and Propagation*, *Conf. Publ. 436*, pp. 1.150–1.155, Inst. of Electr. and Electron. Eng., New York.

Scott, S. L., B. J. Rickett, and J. W. Armstrong (1983), The velocity and the density spectrum of the solar wind from simultaneous three-frequency IPS observations, *Astron. Astrophys.*, *123*, 191–206.

Sovers, O. J., J. L. Fanselow, and C. J. Jacobs (1998), Astrometry and geodesy with radio interferometry: Experiments, models, results, *Rev. Mod. Phys.*, *70*, 1393–1454.

Tanner, A. B., and A. L. Riley (2003), Design and performance of a high-stability water vapor radiometer, *Radio Sci.*, *38*(3), 8050, doi:10.1029/2002RS002673.

Tinto, M. (1996), Spacecraft Doppler tracking as a xylophone detector of gravitational radiation, *Phys. Rev. D*, *53*, 5354–5364.

Tinto, M. (2002), The Cassini Ka-band gravitational wave experiment, *Class. Quantum Gravity*, *19*, 1767–1773.

Tinto, M., and J. W. Armstrong (1998), Spacecraft Doppler tracking as a narrow-band detector of gravitational radiation, *Phys. Rev. D*, *58*, 042002.

Tortora, P., L. Iess, and J. E. Ekelund (2002), Accurate navigation of deep space probes using multifrequency links: The Cassini breakthrough during solar conjunction experiments, paper presented at World Space Congress, Am. Inst. of Aeronaut. and Astronaut., Houston, Tex., 10–19 Oct.

Tortora, P., L. Iess, and R. G. Herrera (2003), The Cassini multifrequency link performance during 2002 solar conjunction, *Proc. IEEE Aerospace Conf.*, *3*, 1465–1473.

Tortora, P., L. Iess, J. J. Bordi, J. E. Ekelund, and D. C. Roth (2004), Precise Cassini navigation during solar conjunctions through multifrequency plasma calibrations, *J. Guidance Control Dyn.*, *27*, 251–257.

Wahlquist, H. D., J. D. Anderson, F. B. Estabrook, and K. S. Thorne (1977), Recent JPL work on gravity wave detection and solar system relativity experiments, *Atti dei Covegni Lincei*, *34*, 335–350.

Won, L., and A. Lee (2001), *JPL Internal Memorandum SCO-01-044 2001*, Pasadena, Calif.

Woo, R., and J. W. Armstrong (1979), Spacecraft radio scattering observations of the power spectrum of electron density fluctuations in the solar wind, *J. Geophys. Res.*, *84*, 7288–7296.

J. W. Armstrong and S. W. Asmar, Jet Propulsion Laboratory, California Institute of Technology, Pasadena, CA 91109, USA. (sami.asmar@jpl.nasa.gov)

L. Iess, Dipartimento di Ingegneria Aerospaziale e Astronautica, Università di Roma "La Sapienza," I-00184 Rome, Italy.

P. Tortora, II Facoltà di Ingegneria, Università di Bologna, I-47110 Forlì, Italy.